Measurement of Vacuum-Assisted Photoionization at 1 GeV for Au and Ag Targets

D. Dauvergne*, A. Belkacem**, F. Barrué*, J. P. Bocquet***, M. Chevallier*, B. Feinberg**, R. Kirsch*, J. C. Poizat*, C. Ray*, and D. Rebreyend***

* Institut de Physique Nucléaire, CNRS/IN2P3, Université Claude Bernard, Lyon I, 4 rue E. Fermi, F-69622 Villeurbanne cedex, France

** Lawrence Berkeley National Laboratory, Berkeley, CA 94720, USA

*** Institut des Sciences Nucléaires, CNRS/IN2P3, Université Joseph Fourier, 53 avenue des Martyrs, F-38026 Grenoble cedex, France

Abstract

We report a measurement of photon impact ionization of K and L-shell of Au and K-shell of Ag targets in the 1-GeV energy range. We show that the cross section is dominated by a contribution from a new channel called vacuum-assisted photoionization. In this process the energy-momentum balance associated with the removal of the inner-shell electron is obtained by conversion of a high-energy photon into an electron-positron pair. This measurement is consistent with the theoretical prediction that vacuum-assisted photoionization is the most probable ionization mechanism at very high energies.

PACS number: 32.80.Fb, 32.80.-t

Inner-shell photoionization of an atom, molecule or ion, is one of the most basic processes in atomic collisions. With several very high energy and high intensity synchrotron x-ray sources existing or being built around the world, the physics of inner-shell photoionization has undergone a significant rebirth in the last two decades [1-3]. Detailed studies of single and double ionization mechanisms, electron correlation effects, post-collision interaction effects have resulted in major advances of our understanding of photoionization mechanisms in the soft and hard x-ray regime. Ionization may proceed through the photoelectric effect or Compton scattering and, in the limit of high energies, the cross section associated with both processes decreases nearly linearly with increasing photon energy [4-5].

The situation is quite different at relativistic energies. When the photon energy exceeds twice the rest mass of the electron, the negative energy continuum will play an additional important role. Photoionization can now proceed through a new channel in which the excess energy is taken by one of the negative-energy continuum electrons [6-7]. The final result is the creation of an inner-shell vacancy (K, L, M,….) along with the creation of an electron-positron pair on the same atom. The recent theoretical work by Ionescu et al. [6] predicted that this new mechanism called vacuum-assisted photoionization (VAP) will become the most probable ionization mechanism for photon energies beyond a few hundreds of MeV. Various mechanisms contribute to the VAP cross section and a detailed discussion of each mechanism can be found in reference [6]. One of the mechanisms that contribute to the total cross section is the well-known triplet production [8]. This latter process is usually calculated as the incoherent part of the pair production process that, in addition to ionization, includes major contributions in which the atom is left in an excited state.

The aim of this paper is to report the first measurement of vacuum-assisted photoionization in the GeV energy range for Au and Ag targets and its comparison to theory. The experimental work is carried out at the European Synchrotron Radiation Facility (ESRF) in Grenoble, France. High energy photons are produced by Compton backscattering of laser photons from the 6 GeV electron beam (GRAAL beam line [9]). The ring is run in 16-bunch mode, leading to a pulsed photon beam. A sketch of the layout is shown in Fig.1. Each backscattered photon is tagged in energy and time by the detection of the scattered electron after deflection inside a bending magnet. The tagging setup consists of an array of plastic scintillators that divide the energy range of the scattered electrons into fifteen intervals. The energy of the backscattered high-energy photon is given as a difference between the initial energy of the electron in the ring and the detected energy of the scattered electron. The "tagged" photon energy distribution ranges from 0.7 to 1.5 GeV with the lower limit of the range given by a geometrical detection cut-off of the tagging system and the higher photon energy limit corresponding to the Compton edge.

A two-slit collimator defines a photon beam spot of 19 mm (horizontal) and 15 mm (vertical) at the target location. A 2-mm thick lead absorber set at the collimator location prevents synchrotron radiation produced in the ring from reaching the target area and creating unwanted background. The lead absorber and the collimation result in an attenuation of about 40% of the Compton backscattered high-energy photon beam. Further cleaning of the high-energy photon beam is achieved by a strong dipole magnet that removes all charged particle created upstream or in the ring.

The expanded onset in Fig. 1 shows some details of the target and detection area. The 2-m target area is kept under primary vacuum of 10^{-3} Torr. A large area thin scintillator (B1) set

1.8 m upstream from the target is used as a veto of any event that involves a charged particle impinging directly on the target. A second magnet further sweeps out of the beam any charged particle created downstream of B1. This combination of cleaning magnets, shielding and veto counters ensures that only photons in the selected energy range impinge on the target. The photon beam intensity is always kept below $3x10^5$ photons/second to avoid fortuitous events caused by multiple incoming photons per pulse.

The high-energy photon beam has a fraction of less than a percent probability to convert into an electron-positron pair in the thin Au and Ag foils. The created high-energy electron and positron fly downstream along the same direction as the initial photon and will deviate by at most a few milliradians from the beam direction. Electron-positron pairs created in the target are detected by a thin scintillator B2. B2 is used to validate the trigger of the pair production in all the measurements presented here and its thickness is chosen in a way to bring the detection efficiency of a charged particle close to unity while keeping the probability of triggering by a high-energy photon to a fraction of a percent. To further discriminate against false triggers by the incident photon beam a thicker (5 mm) plastic scintillator B3 is used to sign the pair creation. At relativistic energies electrons or positrons are minimum ionizing particles and will deposit about 1 MeV in B3 independently of their energy. Two charged particles will lose twice that amount of energy. An amplitude analysis of the response of detector B3 allows the selection of events in which two simultaneous charged particles (e+ and e-) go through it. A calorimeter (B4) made of entangled lead and scintillating fibers with a total absorption length of several radiation lengths is used to collect the total energy deposited by produced e+ and e- particles giving an additional measurement of the incident photon energy.

Electron-positron pair production was extensively studied for the last several decades and a good understanding of the process and agreement for total and partial cross sections with theoretical calculations are achieved. As a check of our experimental technique we first measured electron-positron pair production total cross section in the Au and Ag targets by selecting the two particle events in B3. Figure 2 shows the measured absolute e^+-e^- pair production probabilities for Au and Ag atoms as a function of target foil thickness. Linear fits of the data provide a measured cross section of 35.1 and 14.2 barns for Au and Ag, respectively. Fluctuations of the data around the mean probabilities are very small. These values are in very good agreement with the theoretical values 36.6 and 14.7 barns, respectively [8] when the experimental photon incident energy range is folded in the calculations.

A signature of VAP is given by a simultaneous detection of a K- or L-vacancy in coincidence with the production of an electron-positron pair. Note that, unlike the case of the produced pair, the energy of the ionized-target electron is generally too low [6] to be detected by our experimental set up. The inner-shell vacancy is detected through its characteristic fluorescent K_α or K_β lines when the vacancy is filled. A large area germanium detector (Ge) is used to detect x-rays emitted at the target. We used two methods to calibrate the x-ray detection efficiency of our system. In the first method the x-ray detection efficiency is calculated using x-ray absorption probabilities along the path to the detector, including auto-absorption in the target, fluorescence yields, response efficiency and geometrical efficiency of the Ge detector. In the second method we used Pb foils upstream from the target to produce well-known amounts of electron-positron pairs. We measured inner-shell ionization generated by these pairs in the Au and Ag targets and used tabulated electron impact ionization cross section [10] to deduce the detection efficiency. The two methods give consistent detection

efficiencies for the set up. Figure 3-a shows a typical x-ray spectrum for a Ag target. The corresponding energy spectrum of the particle detector B3 is shown in Fig. 3-b and exhibits well separated peaks for one- and two-particle contributions. Note that the B3 spectrum includes in it the condition that the Ge detector sees a photon as shown in figure 3-a (fluorescent peaks and background). When we require the creation of an inner-shell vacancy in the target by setting a cut on the fluorescent Ag-$K_{\alpha,\beta}$ X-rays the one-electron peak in the B3 spectrum almost vanishes and the spectrum is almost entirely dominated by a two-particle peak (see the dark area in Fig.3) corresponding to the creation an electron-positron pair. The one-electron peak in B3 is correlated mostly to the background seen by the Ge detector and is likely due to Compton scattering in all the surrounding material, including B2, which is much thicker than the target. In contrast the detection of an inner-shell vacancy selects events that took place inside the target. This is a clear signature that inner-shell photoionization is strongly correlated with the creation of an electron-positron pair. Two cases are likely to have happened. i) The inner-shell vacancy and the pair creation take place on the same target atom ii) The inner-shell vacancy and the pair conversion take place on two separate atoms of the target. First the pair is produced in the field of one atom and then the electron or the positron interacts with a different atom resulting in the creation of an inner-shell vacancy. This constitutes a background to our measurement that we will call a two-step process.

The interest here is to extract the contribution of VAP that is the process in which both inner-shell vacancy and pair creation take place on the same atom. In order to do this, we measure, as a function of the target thickness, the probability of creating an inner-shell vacancy (K_{α} and K_{β} for example) in coincidence with the creation of an electron-positron pair (two-particle peak in B3 spectrum). The probability for VAP varies linearly with target thickness while the two-step process varies as the square of the target thickness.

Figure 4 shows the variation of the absolute probabilities for inner-shell vacancy production in coincidence with pair creation for Au (K- and L-shells) and Ag (K-shell), as a function of target thickness. The two-step process dominates for the very thick targets. The measured probabilities are reproduced to better than 5% by theoretical values calculated using tabulated electron-positron cross sections [8] folded with tabulated electron impact ionization cross sections [10]. This provides a further check of the experimental set up. We observe a clear departure from the quadratic dependence shown as dashed lines for all the studied systems. The finite linear term of the fit gives a measure of VAP. We summarize in table I the cross sections extracted from the fits. We also include the pair production cross sections discussed earlier in this paper and the comparison of both processes with theoretical predictions. These experimental results constitute the first absolute measurement of VAP cross section. These values are a factor of 5 to 10 larger than contributions from Compton scattering and photoelectric effect taken from the literature. These measurement are consistent with the prediction that VAP dominates photoionization cross sections at high energies. The theoretical values of VAP shown in table I are deduced from VAP calculations for hydrogenic Ag and Au ions [6]. They include contributions from both the process in which the pair is created on the target electron as well as the process in which the pair is created on the nucleus. These two contributions to VAP are discussed in ref [6]. In particular it is expected that the contribution to VAP cross section for tightly bound Au K-shell comes mainly from the mechanism that involves pair creation on the nucleus. The experimental value of VAP appears to be slightly smaller than theory for Au K-shell and in agreement or slightly larger than theory for Au L-shell and Ag K-shell. This may be an indication that the contribution from VAP that involves pair creation on the nucleus is smaller than predicted by theory. This could be due to e^+/e^- mutual screening at the Au K-shell orbital scale. However the error bars

of our measurement are large and further experimental studies are needed to draw any definitive conclusion on the relative contributions of the two VAP mechanisms.

Acknowledgements

We gratefully thank the GRAAL collaboration for granting us access to the high-energy photon beam. This work is supported by a France-Berkeley grant, by the French CNRS/IN2P3 and by the office of science, office of basic energy sciences, chemical sciences division of the U.S. Department of Energy (DOE) under contract No DE-AC-03-76SF00098.

Figure and Table Captions

Table 1: cross sections per target atom for pair creation and per target shell for vacuum assisted photoionization (VAP). Uncertainties are due to statistics and fitting procedure. An additional 20% systematic error bar has to be accounted for experimental VAP cross sections. Theoretical cross sections are taken from ref. [6]. Compton scattering (CS) and photoelectric effect (Photo) cross sections are taken from ref. [8].

Figure 1 : Experimental setup at the high-energy photon-GRAAL beam line of ESRF. The inset shows details of the target area. B1 to B3 are plastic scintillators, Ge a germanium detector (see text).

Figure 2: Pair creation probability in silver and gold targets

Figure 3: (a) Energy spectrum of x-rays detected in coincidence with a charged particle for a 15.3 $mg.cm^{-2}$ thick Ag target. (b) corresponding amplitude spectrum in the thick scintillator B3. The gray zones of both spectra correspond to the selection of events containing only $K_{\alpha,\beta}$ photons detected by the Ge detector.

Figure 4: Probabilities for K- or L-shell vacancy production in coincidence with pair creation in gold and silver targets. Error bars correspond to statistical and absolute dose determination uncertainties. Solid lines are fits using the sum of a linear and a quadratic function. Dashed lines are the corresponding quadratic functions.

References

[1] J.C. Levin et al, Phys. Rev. Lett. 76 (1996) 1220.

[2] Atomic, Molecular and Optical Physics Handbook, edited by G.W. Drake (AIP, Woodbury, NY, 1996); see section written by Bernd Crasemann, p. 701.

[3] "X-ray and inner-shell processes" edited by P. Lagarde, J. F. Wuilleumier, and J.P. Briand, special issue of J. Phys. (Paris) Colloq. 48 (1987) C9-48.

[4] W. Heitler, "The quantum theory of radiation" (Dover, New York, 1984).

[5] R.H. Pratt, A. Ron, and H. K. Tseng, Rev. Mod. Phys. 45 (1973) 273.

[6] D.C. Ionescu, A. H. Sorensen and A. Belkacem, Phys. Rev. A 59 (1999) 3527.

[7] A. Belkacem, D. Dauvergne, B. Feinberg, H. Gould, D.C. Ionescu and J. Maddi in "x-ray and inner-shell processes", edited by R.W. Dunford, D.S. Gemmell, E.P. Kanter, B. Krassig, S.H. Southworth and L. Young, AIP, Melville, New York 2000, ISBN 1-56396-713-8, p. 153.

[8] J.H. Hubbell, H.A. Gimm, and I. Overbo, J. Phys. Chem. Ref. Data 9 (1980) 1023.

[9] J.-P. Bocquet, Nucl. Phys. A622 (1997) 124c.

[10] J. H. Scofield, Phys. Rev. A 18 (1978) 963.

	Pair creation (barns)	Pair creation theory [8] (barns)	VAP (mbarns)	VAP theory [6] (mbarns)	CS and Photo (mbarns)
Au K-shell	35.1	36.6	8.3 ± 6.2	19.4	2.3
Au L-shell			116 ± 76	42.2	9.3
Ag K-shell	14.2	14.7	18 ± 6	13.2	2.3

Table 1

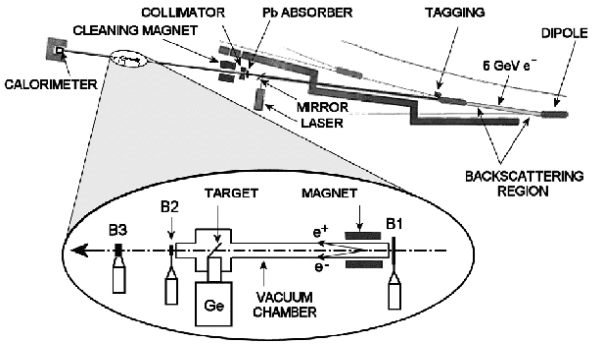
COLLIMATOR
Pb ABSORBER
TAGGING
CLEANING MAGNET
DIPOLE
5 GeV e⁻
CALORIMETER
MIRROR
LASER
BACKSCATTERING
REGION
TARGET
MAGNET
B2
B3
B1
e⁺
e⁻
Ge
VACUUM
CHAMBER

Figure 1

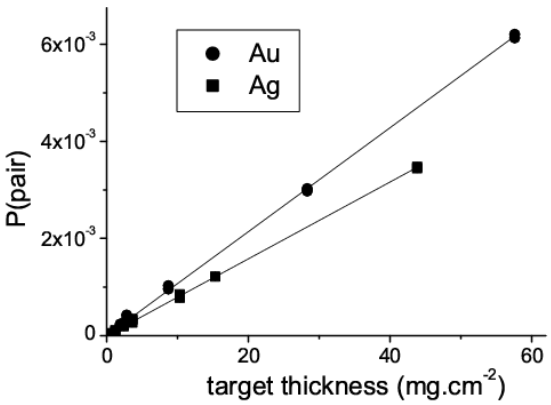
Au
Ag
P(pair)
6x10-3
4x10-3
2x10-3
0
0
20
40
60
target thickness (mg.cm-2)

Figure 2

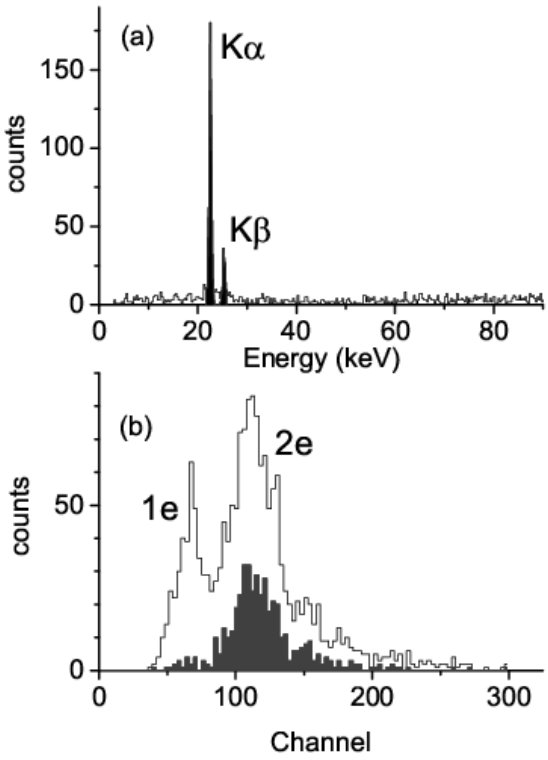
(a)
Kα
Kβ
counts
150
100
50
0
0
20
40
60
80
Energy (keV)
(b)
2e
1e
counts
50
0
0
100
200
300
Channel

Figure 3

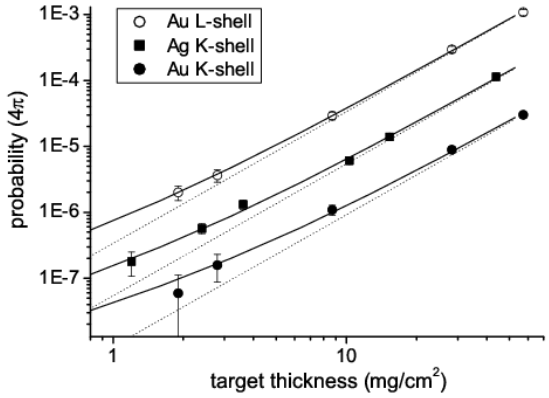
Au L-shell
Ag K-shell
Au K-shell
1E-3
1E-4
1E-5
1E-6
1E-7
probability (4π)
1
10
target thickness (mg/cm²)

Figure 4